International Journal of Modern Science and Technology *Vol. 1, No. 9, December 2016. Page 329-336.*
http://www.ijmst.co/ ***ISSN: 2456-0235.***

Research Article

Synthesis and Characterization of Ternary Pt–Ru–Mo/MC Anode Catalyst on Membraneless Methanol Fuel Cells

P. Ramar[1], M. Chitralekha[2]

[1]Department of Chemistry, Government Arts College, Ariyalur – 621 713. India.
[2]Department of Chemistry, D G Government Arts College, Mayiladuthurai – 609 001. India.

*Corresponding author's e-mail: chitralekhaprof@yahoo.com

Abstract

In the present work, mesoporous carbon-supported Pt–Ru–Mo electrocatalyst for methanol electro-oxidation were synthesized by Bonnemann's method and characterized in terms of their structure, morphology, and composition by using XRD, TEM, and EDX techniques. XRD and EDX results revealed the structural information for alloy catalysts together with their carbon support. TEM measurements revealed a decrease in the mean particle size (5 nm) of the catalysts for the ternary compositions. The structural change was beneficial for the catalytic activity of the compositions. The electrocatalytic activities of $Pt_{34}Ru_{33}Mo_{33}$/MC, $Pt_{50}Ru_{50}$/MC, $Pt_{50}Mo_{50}$/MC, and Pt_{100}/MC catalysts for methanol oxidation in an acid medium were investigated by CV and CA. CA results showed that $Pt_{34}Ru_{33}Mo_{33}$/MC gives a high current under a steady condition. The single membraneless methanol fuel cell performances of the $Pt_{34}Ru_{33}Mo_{33}$/MC, $Pt_{50}Ru_{50}$/MC and $Pt_{50}Mo_{50}$/MC anode catalysts were evaluated at room temperature. Among the catalysts investigated, the power density obtained for $Pt_{34}Ru_{33}Mo_{33}$/MC (34.3 mW cm^{-2}) catalyst was higher than that of $Pt_{50}Ru_{50}$/MC (23.1 mW cm^{-2}) and $Pt_{50}Mo_{50}$/MC (20.3 mW cm^{-2}) using 1.0 M methanol + 0.5 M H_2SO_4 as the anode feed and 0.1 M sodium percarbonate + 0.5 M H_2SO_4 as the cathode feed.

Keywords: Electrocatalysts; Mesoporous carbon; Methanol; Power density; Membraneless methanol fuel cells.

Introduction

The need for more efficient energy conversion systems is presently in great evidence as the world fossil fuel sources become depleted. Fuel cells have shown to be an interesting and very promising alternative to solve the problem of clean electric power generation with high efficiency [1]. The development of new electrocatalyst materials, with significantly lower affinity for carbon monoxide, is essential in the further advancement of membraneless methanol fuel cell (MLMFC) technology. Since platinum is unfortunately extremely susceptible to CO, an ideal catalyst for the anode would be fully tolerant to CO poisoning. Thus the anode should be able to tolerate fuel contaminants and partial oxidation products, which are a main cause of anodic voltage loss. It is well established that bimetallic systems, with Pt as one of the components, can give substantial tolerance to the presence of CO in the fuel stream.

Many efforts have been conducted to improve the lifetime of the methanol fuel cell without increasing cost or losing performance, exploring binary and ternary anode catalysts [2, 3]. The problem of ternary alloys formation is the incessant changes in the morphology during operation that yields new surface compositions with different electrocatalytic abilities towards methanol oxidation. So far, many Pt-based catalysts have been proposed as alternatives to Pt–Ru/MC [4] among them, the bimetallic Pt–Mo/MC alloy catalyst has attracted considerable attention due to their high catalytic performance [5-8].

In this present study, Pt, Pt–Mo, Pt–Ru and Pt–Ru–Mo electrocatalysts supported on mesoporous carbon were synthesized by Bonnemann reduction methods. The prepared catalysts are characterized by dispersive X-ray spectroscopy (EDX), transmission electron microscopy (TEM), X-ray diffractometry (XRD) and electrochemical characterization techniques

Received: 29.11.2016; Received after Revision: 15.12.2016; Accepted: 16.11.2016; Published: 18.12.2016

of cyclic voltammetry (CV), and chronoamperommetry (CA). The catalytic activity of the prepared catalysts toward methanol oxidation has been evaluated in a membraneless methanol fuel cell (MLMFC) as the anode catalysts.

Experimental

Materials

The metal precursors used for the preparation of electrocatalysts were $H_2PtCl_6.6H_2O$ (from Sigma Aldrich), $RuCl_3.3H_2O$ (from Sigma Aldrich) and $MoCl_5$ (from Sigma Aldrich). Mesoporous carbon black (from Cabot Corp.,) was used as a support for the catalysts. Graphite plates (from E-TEK) were used as substrates for the catalyst to prepare the electrodes. Nafion® (DE 521, DuPont USA) dispersion was used to make the catalyst slurry. Tetrahydrofuran (THF) (from Merck) was used as a solvent. Methanol (from Merck), sodium percarbonate (from Riedel) and H_2SO_4 (from Merck) were used as the fuel, the oxidant and as the electrolyte for electrochemical analysis, respectively. All the chemicals were of analytical grade. Pt/MC (40-wt%, from E-TEK) was used as the cathode catalyst.

Catalyst preparation

The Pt–Ru–Mo/MC (1:1:1%) electrocatalysts were prepared by a colloidal process known as the Bonnemann's method [9-10]. The Bonnemann method was chosen as crystallite sizes between 1.5 and 2.5 nm can be obtained, showing enhanced electrocatalytic activities due to their favorable surface-to-bulk ratio. First NR4X (tetraalkylammonium-X) stabilized colloidal precursors (where X is the electrocatalyst particle) were prepared via the reduction of anhydrous $H_2PtCl_6.6H_2O$, $RuCl_3.3H_2O$ and $MoCl_5$ dissolved in THF tetrahydrofuran. Then a suspension of mesoporous carbon (from Cabot Corp.,) in ultrapure water (Millipore MilliQ, 18 MΩ cm), was impregnated with the appropriate amount of the colloidal solution.

Thermal treatments were carried out in a H_2 reducing atmosphere at 300°C for 120 min. For comparison, the monometallic Pt/MC, bimetallic Pt–Ru/MC and Pt–Mo/MC catalysts were synthesized under the same conditions. The electrocatalytic mixtures and atomic ratios were $Pt_{34}Ru_{33}Mo_{33}$/MC, $Pt_{50}Ru_{50}$/MC, $Pt_{50}Mo_{50}$/MC, and Pt_{100}/MC. The nominal loading of metals in the electrocatalysts was 40 %wt. and rest 60 %wt. was mesoporous carbon.

Physical characterization

The morphology of the dispersed catalysts was examined using SEM (ZEISS EVO 50 Scanning Electron Microscope) and TEM (Philips CM 12 Transmission Electron Microscope). The particle size distribution and mean particle size were also evaluated using TEM. The crystal structure of the synthesized electrocatalysts was characterized by powder X-ray diffraction (XRD) using a Rigaku multiflex diffractometer (model RU-200 B) with Cu-$K_{\alpha 1}$ radiation source ($\lambda_{K\alpha 1}$ = 1.5406 A^o) operating at room temperature. The tube current was 40 mA with a tube voltage of 40 kV. The 2θ**Error! Reference source not found.** angular regions between 20º and 90º were recorded at a scan rate of 5° min^{-1}. The mean particle size analyzed from TEM is verified by determining the crystallite size from XRD pattern using Scherrer formula. Pt (2 2 0) diffraction peak was selected to calculate crystallite size and lattice parameter of platinum. According to Scherrer's equation shown in Eq. (1),

$$d = \frac{0.9\lambda_{K\alpha 1}}{ß_{2\theta} \cos \theta_{max}} \qquad (1)$$

where d is the average crystallite size, θ_{max} is the angle at the position of the peak maximum, $ß_{2\theta}$ is the width of the peak (in radians), 0.9 is the shape factor for spherical crystallite and $\lambda_{K\alpha 1}$ is the wavelength of X-rays used. The lattice parameters of the catalysts were estimated according to Eq. (2).

$$a = \frac{\sqrt{2}\,\lambda_{K\alpha 1}}{\mathrm{Sin}\,\theta_{max}} \qquad (2)$$

where, 'a' is the lattice parameter (nm) and all the other symbols have the same meanings as in Eq. 2. The atomic ratio of the catalysts was determined by an energy dispersive X-ray (EDX) analyzer, which was integrated with the TEM instrument.

Electrochemical measurements

The electrochemical experiments were carried out in a conventional three-electrode cell

at room temperature. Voltammetric curves using 0.5 M H_2SO_4 or 1 M CH_3OH/0.5 M H_2SO_4 electrolyte solutions purged with nitrogen gas were recorded with an electrochemical workstation (CHI-6650; CH Instruments, USA). Catalyst coated glassy-carbon electrode was used as the working electrode and a platinum wire was used as the counter electrode. Ag/AgCl in saturated KCl was used as the reference electrode. The activity of the electrocatalysts was determined by cyclic voltammetry in a half cell at a scan rate of 50 mVs^{-1} between 0.05 and 1.2 V vs. Ag/AgCl and chronoamperometry (0.4 V vs. Ag/AgCl for 30 min).

Results and discussions

Physical Characterization

X-ray Diffraction

The XRD patterns of the prepared $Pt_{34}Ru_{33}Mo_{33}$/MC, $Pt_{50}Ru_{50}$/MC, $Pt_{50}Mo_{50}$/MC and Pt_{100}/MC catalysts are shown in Fig. 1. The first peak located at around 25° in all the XRD patterns is attributable to the mesoporous carbon support. The binary and ternary alloy catalysts were shifted to the higher angle side with different amounts because of differences in the atomic percentages of Ru and Mo, compared to that of pure Pt at 2θ values of 39°, 47°, 67° and 82° and are indexed with planes (1 1 1), (2 0 0), (2 2 0) and (3 1 1), respectively, indicating a lattice contraction and alloy formation. These results also indicate that the Pt nanoparticles could be homogeneously alloyed with Ru and Mo. No diffraction peaks were attributed to pure Ru, Mo or to their oxides were observed. The fcc lattice parameters were evaluated from the angular position of the (2 2 0) peaks, which reflect the formation of a homogeneous alloy particles. The lattice parameters obtained for the Pt–Mo/MC (0.3888 nm), Pt–Ru/MC (0.3901 nm) and Pt–Ru–Mo/MC (0.3897 nm) catalysts are smaller than those for Pt/MC electrocatalyst (0.3915 nm) (Table 1). It indicates that, the decrease in lattice parameters of the alloy catalysts results from the progressive increase in the incorporation of Ru and Mo into the alloyed state.

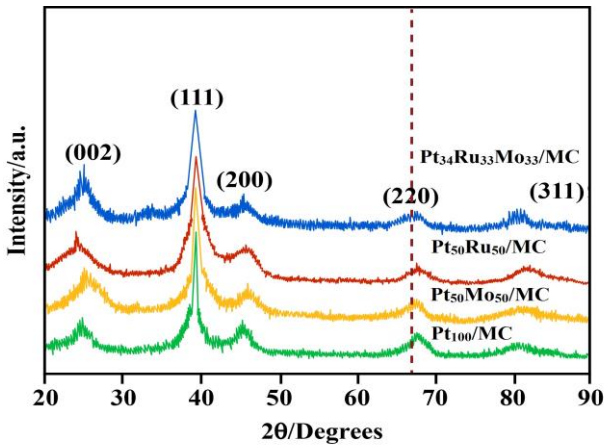

Fig. 1. X-ray diffraction patterns of $Pt_{34}Ru_{33}Mo_{33}$/MC, $Pt_{50}Ru_{50}$/MC, $Pt_{50}Mo_{50}$/MC, and Pt_{100}/MC catalysts

The difference of lattice parameters and the shift of (2 2 0) plane indicate interactions between Pt, Ru and Mo. The average particle size for Pt–Ru/MC, Pt–Mo/MC and Pt–Ru–Mo/MC electrocatalysts were in the range of 1.5-3 nm was estimated using the Scherrer equation are in good agreement with the TEM images.

Table 1. The EDX composition, lattice parameters, and the particle size obtained for different atomic ratios of electrocatalysts

Electrocatalyst	Nominal Atomic ratio			EDX Atomic ratio			Lattice parameter (nm)	Crystallite size (nm)	Particle size from TEM (nm)
	Pt	Ru	Mo	Pt	Ru	Mo			
Pt/MC	100	-	-	99	-	-	0.3915	4.0	3.6
Pt–Mo/MC	50	-	50	51	-	49	0.3883	3.7	3.2
Pt–Ru/MC	50	50	-	52	48	-	0.3901	3.4	3.0
Pt–Ru–Mo/MC	34	33	33	36	32	32	0.3888	3.0	2.8

Transmission Electron Microscopy

TEM image of the $Pt_{34}Ru_{33}Mo_{33}$/MC alloy catalysts and the corresponding particle size distribution histogram are presented in Fig. 2. Narrower particle size distribution was observed with an average particle diameter of 1.5 nm, which is in fairly good agreement with the data calculated from XRD. Nanoparticles are homogenously distributed over the mesoporous carbon support, with no evidence for particle agglomeration. The particle size distribution of

these catalysts is shown in Table 1 in accordance to the TEM images.

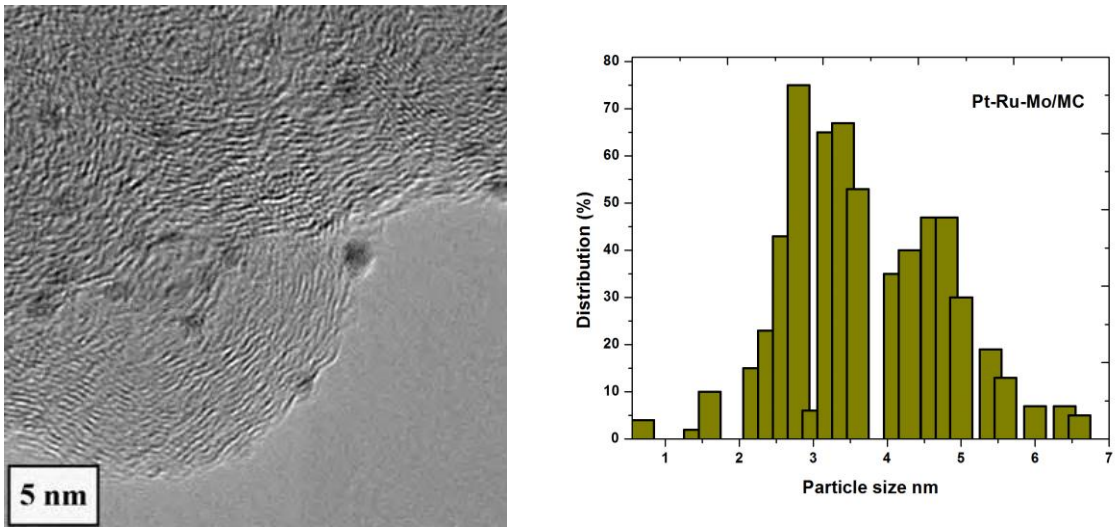

Fig. 2 TEM image and particle size distribution of $Pt_{34}Ru_{33}Mo_{33}$/MC catalyst

Energy Dispersive X-ray Spectroscopy

Energy dispersive X-ray spectroscopy is conducted by focusing the electron beam on several different selected regions of the mesoporous carbon supported nanoparticles. EDX spectrums of Pt–Ru–Mo/MC nanoparticles are shown in Fig. 3. The average composition of the sample was in atom ratio of Pt:Ru:Mo = 1:1:1. The EDX results of the binary Pt–Ru/MC and Pt–Mo/MC and the ternary Pt–Ru–Mo/MC catalysts are very close to the nominal values, which indicate that the metals were loaded onto the carbon support without obvious loss.

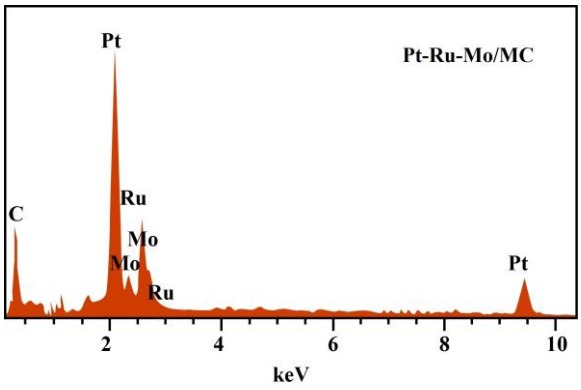

Fig. 3. EDX spectra of Pt–Ru–Mo/MC catalysts

Electrochemical characterization

Cyclic Voltammetry

Fig. 4a shows the cyclic voltammogram (CV) on the $Pt_{34}Ru_{33}Mo_{33}$/MC, $Pt_{50}Ru_{50}$/MC, $Pt_{50}Mo_{50}$/MC and Pt_{100}/MC catalysts for CO oxidation in a solution of 0.5 M H_2SO_4. Due to the strong adsorption of CO onto the Pt surface, the hydrogen adsorption-desorption of the Pt was completely blocked in the hydrogen region; indicating the presence of a saturated CO adlayer [11]. The electrochemically active surface areas (SEAS) of the electrocatalyts were calculated by using Eq. (3) [12-14]. S_{EAS} values were estimated using hydrogen adsorption/desorption charge ($S_{EAS/H}$), and roughness of electrodes.

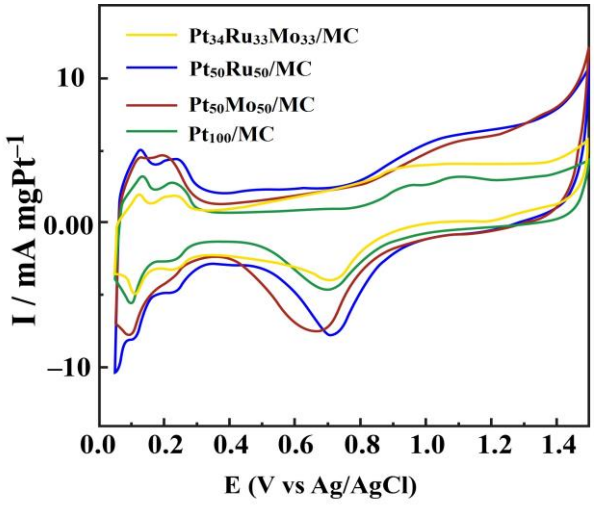

Fig. 4a. CVs of $Pt_{34}Ru_{33}Mo_{33}$/MC, $Pt_{50}Ru_{50}$/MC, $Pt_{50}Mo_{50}$/MC and Pt_{100}/MC electrocatalysts in 0.5 M H_2SO_4.

$$S_{EAS/H}(m^2/g) = \frac{Q_H(\mu C/cm^2)/\mu 2)}{210(\mu C/cm^2) \times 0.77 \times [Pt]} \quad (3)$$

Where Q_H is the charge corresponding to desorption of hydrogen on the Pt surface, [Pt] (mg/cm^2) is the Pt loading on the electrode surface, 210 μC/real cm^2 is the charge required to oxidize a monolayer of hydrogen on the Pt surface, 0.76 is the hydrogen monolayer coverage [15]. Estimation of the electrode roughness and S_{EAS} values are shown in Table 2.

Based on these values, the highest electrochemically active area is achieved for the ternary electrocatalysts.

Table 2. Comparison of hydrogen desorption charge and carbon monoxide desorption charge, and its electrochemical active surface area (S_{EAS}) and electrode roughness

Catalyst	Q_H/μC	Electrode real surface area (cm^2)	$S_{EAS/H}$ (m^2gPt^{-1})[a]	Roughness
Pt_{100}/MC	437	2.1	27	58.7
$Pt_{50}Mo_{50}$/MC	233	1.0	28	30.7
$Pt_{50}Ru_{50}$/MC	250	1.1	30	33.5
$Pt_{34}Ru_{33}Mo_{33}$/MC	197	0.8	35	25.1

The CV curves were obtained in a half cell between 0.05 and 1.2 V (vs. Ag/AgCl) in the absence of methanol. The characteristic features of polycrystalline Pt, i.e. hydrogen adsorption/desorption peaks in low potential region, oxide formation/stripping wave/peak in high potential region and a flat double layer in between, are observed for all the synthesized catalysts. The voltammograms of the electrocatalysts did not display a well-defined hydrogen region between 0.05 and 0.35 V, as the catalyst's features in this region are influenced by their surface composition. A considerable increase in the voltammetric charge of ternary $Pt_{34}Ru_{33}Mo_{33}$/MC catalyst was observed in the double-layer region, indicating that the addition of Mo into binary Pt–Ru/MC leads to an enhanced activity for the oxidation reactions.

Fig. 4b corresponds to representative CVs of methanol oxidation under acidic conditions (1.0 M CH_3OH and 0.5 M H_2SO_4) catalyzed by $Pt_{34}Ru_{33}Mo_{33}$/MC, $Pt_{50}Ru_{50}$/MC, $Pt_{50}Mo_{50}$/MC and Pt_{100}/MC catalysts. The onset potential for the oxidation of methanol in a positive scan was a key factor for evaluating the catalyst activity [16]. The onset potentials for the oxidation of methanol on the $Pt_{34}Ru_{33}Mo_{33}$/MC (0.34 V) electrocatalysts is slightly lower than that on the $Pt_{50}Ru_{50}$/MC (0.38 V), $Pt_{50}Mo_{50}$/MC (0.40 V) and Pt_{100}/MC (0.49 V) catalysts. All the current values were normalized by the geometric surface area of the electrode used. The CV curves depict the presence of a peak in the potential range of the positive sweep and another peak in the negative sweep. The peak in the positive sweep is associated with the methanol oxidation, and the peak in the negative sweep is related to the oxidation of carbonaceous intermediate products from incomplete methanol oxidation.

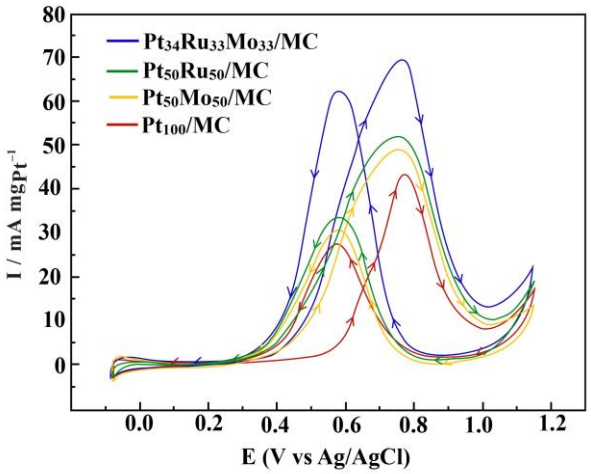

Fig. 4b. CVs of $Pt_{34}Ru_{33}Mo_{33}$/MC, $Pt_{50}Ru_{50}$/MC, $Pt_{50}Mo_{50}$/MC and Pt_{100}/MC electrocatalysts in 1.0 M methanol + 0.5 M H_2SO_4

Table 3. CV results of $Pt_{34}Ru_{33}Mo_{33}$/MC, $Pt_{50}Ru_{50}$/MC, $Pt_{50}Mo_{50}$/MC and Pt_{100}/MC electrocatalysts

Catalyst	Positive peak potential (mV vs. Ag/AgCl)	Scan rate 50 mV s^{-1} Peak current density (mA/cm^2)
Pt_{100}/MC	787	40.2
$Pt_{50}Mo_{50}$/MC	785	47.1
$Pt_{50}Ru_{50}$/MC	786	49.0
$Pt_{34}Ru_{33}Mo_{33}$/MC	788	68.1

The peak current densities of $Pt_{34}Ru_{33}Mo_{33}$/MC, $Pt_{50}Ru_{50}$/MC, $Pt_{50}Mo_{50}$/MC and Pt_{100}/MC catalysts are 68.1, 49.0, 47.1 and 40.2 mA/cm^2, respectively, showing that the activity of the ternary $Pt_{34}Ru_{33}Mo_{33}$/MC catalyst is a factor of ~1.5 times higher than that of the Pt/MC catalyst. Table 6.3 summarizes the CV

results of $Pt_{34}Ru_{33}Mo_{33}$/MC, $Pt_{50}Ru_{50}$/MC, $Pt_{50}Mo_{50}$/MC and Pt_{100}/MC electrocatalysts including the positive peak potentials and the corresponding peak current densities of MOR.

The CV results show that pure Pt_{100}/MC catalysts do not behave as an appropriate anode for MOR due to its poisoning by strongly adsorbed intermediates such as CO. However, the introduction of Ru and Mo promotes the electrocatalytic activity. CV for methanol oxidation reactions showed that the CO poisoning effect was largely inhibited by $Pt_{34}Ru_{33}Mo_{33}$/MC electrocatalysts, indicating the ability of Mo to promote either the CO to CO_2 oxidation or a weaker adsorption of CO on the $Pt_{34}Ru_{33}Mo_{33}$/MC catalysts.

Chronoamperometry

Fig. 5 shows the current densities measured from 0.05 to 1.2 V in 1.0 M methanol+0.5 M H_2SO_4. The currents decay with time in a parabolic style and reach an apparent steady state within 80s.

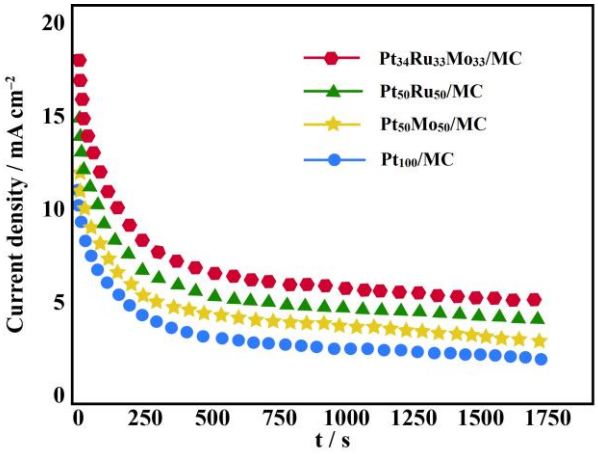

Fig. 5. CA of $Pt_{34}Ru_{33}Mo_{33}$/MC, $Pt_{50}Ru_{50}$/MC, $Pt_{50}Mo_{50}$/MC and Pt_{100}/MC electrocatalysts

It can be seen that the current density of methanol electro-oxidation on the $Pt_{34}Ru_{33}Mo_{33}$/MC catalyst is higher than that on the $Pt_{50}Ru_{50}$/MC, $Pt_{50}Mo_{50}$/MC and Pt_{100}/MC catalyst at the same potentials. The activity change for methanol oxidation decreases in the order of $Pt_{34}Ru_{33}Mo_{33}$/MC > $Pt_{50}Ru_{50}$/MC > $Pt_{50}Mo_{50}$/MC > Pt_{100}/MC, which is in fairly good agreement with our CV results. For the durability test, the chronoamperometric experiments were carried out at 0.05 to 1.2 V for 1750 s in the same conditions. Before each measurement, the solution was purged with high-purity nitrogen gas for at least 30 min to ensure oxygen-free measurements.

Single cell performance

A single cell performance was tested using $Pt_{34}Ru_{33}Mo_{33}$/MC, $Pt_{50}Ru_{50}$/MC, $Pt_{50}Mo_{50}$/MC and Pt_{100}/MC electrocatalysts as the anode. Polarization curves and power densities are shown in Fig. 6.

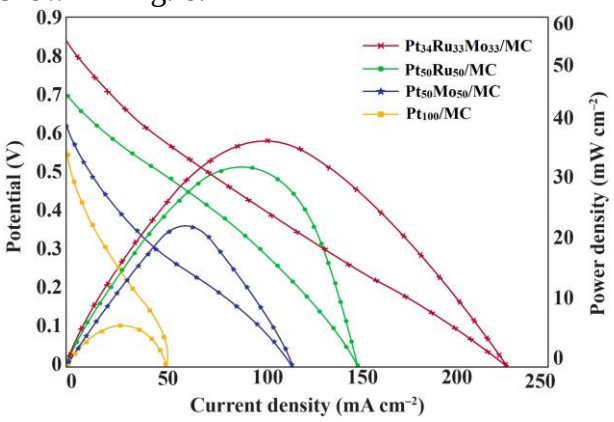

Fig. 6. Polarization and power density curves of $Pt_{34}Ru_{33}Mo_{33}$/MC, $Pt_{50}Ru_{50}$/MC, $Pt_{50}Mo_{50}$/MC and Pt_{100}/MC electrocatalysts

For each catalyst, the open-circuit voltages (OCV) were different, as would be expected in onset potentials. The OCVs of $Pt_{34}Ru_{33}Mo_{33}$/MC, $Pt_{50}Ru_{50}$/MC, $Pt_{50}Mo_{50}$/MC, are higher than that of Pt_{100}/MC, 0.53 V, and the order of OCV is exactly same as the onset potentials. The OCV of $Pt_{34}Ru_{33}Mo_{33}$/MC is the highest value of 0.83 V, which is approximately 0.30 V higher than that of Pt_{100}/MC. This indicates that Pt_{100}/MC is more rapidly poisoned by CO than any other alloy catalyst and that the oxidation of adsorbed CO is enhanced by the second or third metal. In the case of $Pt_{34}Ru_{33}Mo_{33}$/MC the overall performance is superior to that of the bimetallic electrocatalysts. The maximum power densities obtained for $Pt_{34}Ru_{33}Mo_{33}$/MC, $Pt_{50}Ru_{50}$/MC, $Pt_{50}Mo_{50}$/MC and Pt_{100}/MC are 36.5, 30.3, 21.2 and 5.7 mW cm^{-2}, respectively (Table 4). We conclude that the substitution of a small amount of Mo for Ru aids in cleaning surfaces poisoned by CO and provides additional reaction sites for methanol oxidation.

In membraneless fuel cells, pure Pt/MC catalyst does not behave as a very good anode for methanol electro-oxidation due to its poisoning by strongly adsorbed intermediates such as CO. But the addition of Mo to Pt (Pt–

Mo/MC) had a little effect, whereas addition of Mo to Pt–Ru/MC greatly enhanced the electrocatalytic activity. Therefore the results demonstrated that the performance of the developed membraneless fuel cell enhanced profoundly as mentioned in our earlier study [17, 18], if the concentration of oxidant in cathodic stream is 10 times larger, and the current density is also increased approximately ten times.

Table 4. Summary of performance of single fuel cell tests using (2 mg cm^{-2} catalyst loading, 40 wt% catalyst on carbon)

Anode catalysts	Open circuit Voltage (V)	Maximum power density (mW cm^{-2})	Maximum current density (mA cm^{-2})
Pt_{100}/MC	0.53	5.7	49.7
$Pt_{50}Mo_{50}$/MC	0.61	21.2	111.5
$Pt_{50}Ru_{50}$/MC	0.69	30.3	149.8
$Pt_{34}Ru_{33}Mo_{33}$/MC	0.83	36.5	226.0

Conclusions

In present work, the study of methanol oxidation on mesoporous carbon-supported Pt–Ru–Mo ternary nanoparticles has revealed details concerning the activity and stability of the catalysts in membraneless fuel cells. The maximum activity for methanol oxidation was found for the $Pt_{34}Ru_{33}Mo_{33}$/MC than the $Pt_{50}Ru_{50}$/MC, $Pt_{50}Mo_{50}$/MC and Pt_{100}/MC. The significantly enhanced catalytic activity for methanol oxidation can be attributed to the high dispersion of ternary catalysts and to Mo acting as a promotion agent. XRD results show the homogenous alloy structure of Pt, Ru and Mo. The TEM images indicated an average size of $Pt_{34}Ru_{33}Mo_{33}$/MC nanoparticles of 1.5 nm. The atom ratio of Pt, Ru and Mo from EDX analyses is close agreement with the original precursor concentration. The composition of ternary $Pt_{34}Ru_{33}Mo_{33}$/MC nanoparticles can be conveniently controlled by adjusting the initial metal salt solution and preparation conditions. The electrochemical experiments showed that the $Pt_{34}Ru_{33}Mo_{33}$/MC nanoparticles have higher catalytic activity than that of the other catalysts. We expect that the MLMFC may be a promising candidate for practical fuel cells to establish a clean and sustainable energy future. Further work is necessary to characterize the catalysts using different surface analysis techniques and to conduct tests of these electrocatalysts in microfluidic membraneless fuel cells.

Conflict of interest

Authors declare there are no conflicts of interest.

References

[1] Kalaikathir SPR, Begila S. Synthesis and characterization of nanostructured carbon-supported Pt electrocatalysts for membraneless methanol fuel cells. International Journal of Modern Science and Technology. 2016;1:199-212.

[2] Vijayaramalingam K, Kiruthika S, Muthukumaran B. Promoting Effect of Third Metal (M = Ni, Mo and Rh) on Pd–Ir Binary Alloy Catalysts in Membraneless Sodium Perborate Fuel Cells. International Journal of ModernScience and Technology. 2016;3:257-263.

[3] Cao J, Du C, Wang SC, Mercier P, Zhang X, Yang H. The production of a high loading of almost monodispersed Pt nanoparticles on single-walled carbon nanotubes for methanol oxidation. Electrochem Commun. 2007;9:735-740.

[4] Liu H, Song C, Zhang L, Zhang J, Wang H, Wilkinson DP. A review of anode catalysis in the direct methanol fuel cell. J Power Sources. 2006;155:95-102.

[5] Mukerjee S, Lee SJ, Ticcianelli E, McBreen J, Grur BN, Markovic NM. Investigation of enhanced CO tolerance in proton exchange membrane fuel cells by carbon supported PtMo alloy catalyst. Electrochem Solid State Lett. 2 (1999) 12-19.

[6] Neto AO, Franco EG, Arico E, Linardi M, Gonzalez ER, Electro-oxidation of methanol and ethanol on Pt-Ru/C and Pt-Ru-Mo/C electrocatalyst prepared by bonnemann's method. Journal of the European Ceramic Society. 2003;23:2987-2992.

[7] Oetjen HF, Schmidt VM, Stimming U, Trila F. Performance data of a proton exchange membrane fuel cell using H2/CO as fuel

gas. J Electrochem Soc. 1996;143:3838-3842.

[8] Gotz M, Wendt H. Binary and ternary anode catalyst formulations including the elements W, Sn and Mo for PEMFCs operated on methanol or reformate gas. Electrochimica Acta. 1998;43:3637-3644.

[9] Beyhan S, Leger JM, Kadırgan F. Pronounced synergetic effect of the nano-sized PtSnNi/C catalyst for methanol oxidation in direct methanol fuel cell. Applied Catalysis B: Environmental. 2013; 130:305-313.

[10] Radmilovic V, Gasteiger HA, Ross Jr. PN. Structure and chemical composition of a supported Pt-Ru electrocatalyst for methanol oxidation. J Catal. 1995;154:98=106.

[11] Rashidi R, Dincer I, Naterer GF, Berg P, Performance evaluation of direct methanol fuel cells for portable applications. J Power Sources. 2009;187:509-515.

[12] Zhou Z, Wang S, Zhou W, Wang G, Jiang L, Li W. Pt based anode catalysts for direct ethanol fuel cell. Chem Commun. 2003;46:394-395.

[13] Watanabe M, Horiuchi M, Motoo S. Electrocatalysis by ad-atoms: Part XXIII. Design of platinum ad-electrodes for formic acid fuel cells with ad-atoms of the IVth and the Vth groups. Journal of Electroanalytical Chemistry and Interfacial Electrochemistry. 1988;250:117-125.

[14] Cooper JS, McGinn PJ. Combinatorial screening of thin film electrocatalysts for a direct methanol fuel cell anode. J Power Sources. 2006;163:330-338.

[15] Choi SM, Kim JH, Jung JY, Yoon EY, Kim WB. Pt nanowires prepared via a polymer template method: Its promise toward high Pt-loaded electrocatalysts for methanol oxidation. Electrochimica Acta. 2008;53:5804-5811.

[16] Gowdhamamoorthi M, Arun A, Kiruthika S, Muthukumaran B. Perborate as novel fuel for enhanced performance of membraneless fuel cells. Ionics. 2014;20:1723-1728.

[17] Ponmani K, Durga S, Arun A, Kiruthika S, Muthukumaran B. Development of Membraneless Sodium Perborate Fuel Cell for Media Flexible Power Generation. International Journal of Electrochemistry. 2014;2014:1-9.

[18] Mahendran S, Anbuselvan C, Kinetics and mechanism of oxidation of 5-(4'-bromophenyl)-5-oxopentanoic acid by acid permanganate, International Journal of ModernScience and Technology. 2016;3: 106-110.

[19] Priya M, Elumalai M, Kiruthika S, Muthukumaran B. Influences of supporting materials for Pt-Ru binary catalyst in Ethanol fuel cell. International Journal of ModernScience and Technology. 2016;1:5-11.

****

